Journal of Applied Polymer Science

Morphology, structure, and properties of metal oxide/polymer nanocomposite electrospun mats

Natalia Hoogesteijn von Reitzenstein,[1] Xiangyu Bi,[1] Yu Yang,[1] Kiril Hristovski,[2] Paul Westerhoff[1]
[1]School of Sustainable Engineering and the Built Environment, Arizona State University, Tempe, Arizona 85287-3005
[2]The Polytechnic School, Arizona State University, Tempe, Arizona 85287-3005
Correspondence to: N. H. von Reitzenstein (E-mail: natreitzen@asu.edu)

ABSTRACT: Adding nanoparticles into polymer solutions before electrospinning creates unique hierarchical morphologies dispersed throughout small diameter nanoparticle-polymeric fibers. Effects of polymer composition, nanoparticle (NP) type, loading, and electrospinning voltage conditions were studied. As examples, indium, iron, and titanium oxide engineered nanoparticles (NPs) were dispersed into polyvinylpyrrolidone or polystyrene and electrospun. NP loadings below 5 wt % did not affect critical voltage required for Taylor cone formation, whereas higher NP loadings require higher critical voltages. Polymeric fiber thickness and macroscopic morphology is not impacted by up to 5 wt % NP loadings, and NP dispersion throughout the fibers were similar to their dispersion in initial polymer suspension. NP loadings above 5 wt % increased viscosity, which decrease subsequent fiber diameter. Experiments in water containing inorganic and organic pollutants in water demonstrate that the polymer is largely nonporous. This work enables design of multifunctional nanomaterial-polymer composite fibers for wide-ranging applications such as water and air treatment.
 J. Appl. Polym. Sci. **2016**, *133*, 43811.

KEYWORDS: electrospinning; fibers; nanocrystals; nanoparticles; nanowires

Received 5 January 2016; accepted 15 April 2016
DOI: 10.1002/app.43811

INTRODUCTION

Electrospun polymer fibers with diameters in the submicron to nanometer range have unique characteristics that led to increasing interest in their applications as reinforcements for composite materials, air or water filtration, soft tissue prostheses, wound dressing, cosmetics, protective clothing, and sensors.[1,2] Electrospinning uses an electrically charged jet of polymer solution to produce polymer filaments by applying a high voltage potential between 10–40 kV and a grounded collector. The surface tension on the fluid droplet at the syringe tip is overcome by the strength of the electric field and a charged jet of fluid stretches from the syringe tip and deposits onto the grounded collector, forming a mat of fibers with diameters in the micrometer and nanometer scales. Nanoparticle (NP) addition into polymers produces nanocomposites known to improve mechanical strength, resistance to wear, and thermal stability.[3] Additionally, NP-polymer electrospun fiber composites also enhance the fiber performance due to the multifunctionality of NPs as biocides, sorbents, and photocatalysts. As NP-polymer composites are being synthesized, limited information across multiple NP types exists regarding impacts of NPs on polymer spinning behavior.

Synergistic effects of physical parameters dictate the structure and morphology of electrospun fibers.[4] The electrospinning process is a balance of parameters including, but not limited to, conditions such as relative humidity, polymer weight, distance between capillary tip and collector plate, feed rate of solution, and solution composition.[5–7] For example, adjusting the relative humidity in the environment affects the number, diameter, shape, and distribution of pores on the surface of electrospun fibers.[5] Electrostatically, there is a balance between the induced charge on the polymer surface and the surface tension of that polymer. Surface tension is overcome by applying voltage. Viscosity dictates whether the polymer jet will break into droplets or travel as a continuous stream to the collector plate. High viscosity liquids will become jets, while low viscosity liquids will break up.[4] By altering physical parameters and manipulating electrostatic forces, the fibers produced by electrospinning can have a variety of morphologies suited to different purposes. For example, fiber diameter may be manipulated via solution viscosity and applied voltage. Depending on the final use of electrospun fiber mats (i.e., nonwoven textiles), controlling fiber diameter can be controlled. In this work, fiber diameter is shown to vary as an effect of NP addition. The addition of NP

Additional Supporting Information may be found in the online version of this article.

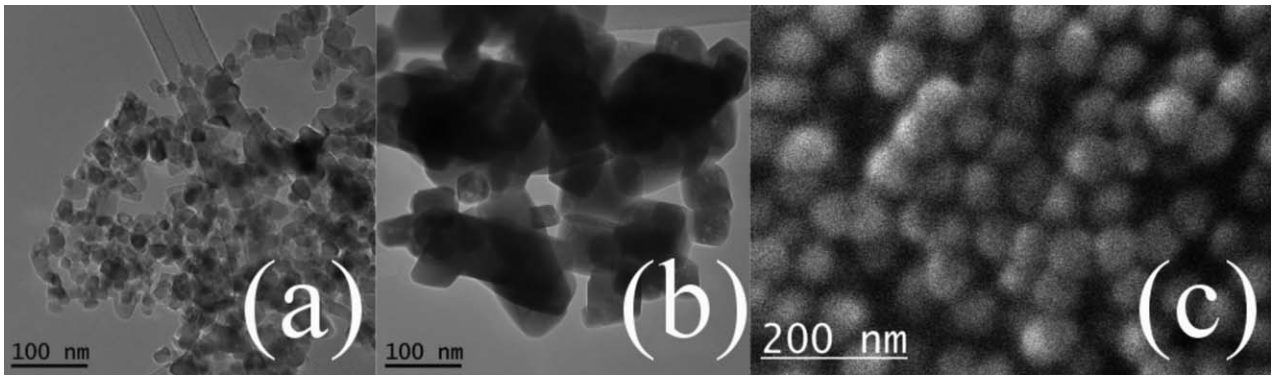

Figure 1. TEM Images of (a) TiO_2, (b) In_2O_3, and (c) Fe_2O_3 nanoparticles utilized for fiber hybridization.

into solution adds another dimension to the process and its product. There are few examples in the literature of the effect of NP addition to polymer solutions prior to spinning and few investigations of the effect of NP on electrospinning process parameters.[8,9] The effect of NP content on the formation of a Taylor cone in polymer solutions for electrospinning presents a gap in the literature that is important for future investigations of electrospun fibers using NPs for functionalization.

Interest exists in coupling the benefits of metal oxide nanoparticles with the process of electrospinning, affording several applications of economically produced, micrometer and nanometer-scale fibers.[10] For example, adding antimicrobial silver NP to a mat of electrospun fibers grafted onto a membrane could help prevent bacterial membrane fouling.[11] Electrospinning polymeric fibers for water treatment applications requires use of nonwater soluble polymers, and hence dissolution in nonaqueous solvents is required. Titanium dioxide (TiO_2) is an inexpensive and effective photocatalyst and chemical sensor in environmental remediation, photovoltaics, and optics, and applications for electrospun fibers made with TiO_2 are beginning to be explored.[12–15] Research on interactions of individual metal oxide nanoparticles with polymers during electrospinning have begun. For example, varying weight percentages of TiO_2 in a polyaniline solution affected nanocomposite fiber diameter, while operating parameters such as TiO_2 loading content, humidity, and temperature affected the physical properties, such as strength and brittleness, of electrospun polyacrylonitrile (PAN)-TiO_2 fibers.[8,9] Less has been reported about the systematic influence of NP addition to polymer solutions on electrospinning parameters (e.g., solution viscosity) and resulting critical voltage or implications for fiber morphology.

This study investigated hybridizing electrospun fibers with NP and evaluated how the NP addition influenced polymer properties, electrospinning conditions, and electrospun fiber morphology. Specifically, we quantified the differences in critical voltage needed to produce an unstable and stable Taylor cone by loading two polymer solutions with different NP weight percentages. Voltage was slowly increased until a stable Taylor cone was observed. Nanoparticle-polymer composite solution viscosity was tested using rheometry. Metal oxide nanoparticles (TiO_2, indium oxide (In_2O_3), hematite (Fe_2O_3) and electrospun polymeric fibers where characterized using transmission electron microscopy (TEM) and energy dispersive X-ray analysis (EDX). TiO_2 was chosen because of its widespread use as a photocatalyst and arsenic absorbent, while In_2O_3 was chosen due to its use in semiconductor industries plus its visual color observation ability and high sensitivity of morphology using scanning electron microscopy (SEM) in order to observe NP distribution in the fibers. Fe_2O_3 was chosen because it is a good adsorbent of inorganic pollutants (such as arsenic) in drinking water. The results are intended to aid in optimization of electrospinning nanocomposites by showing how adding different NP mass fractions can affect viscosity, voltage, surface morphology, and diameter of fibers.

EXPERIMENTAL

Materials

Two polymers (Polyvinylpyrrolidone [PVP] K90 (MW 360,000 g/mol, Fluka Analytical) and Polystyrene (PS, MW 350,000 g/mol, Aldrich Chemistry) were used for electrospinning. These polymers were chosen based on their high molecular weights suitable for electrospinning. N,n-dimethylformamide (DMF, Sigma-Aldrich) was used as the organic solvent to dissolve both of the polymers.

Nanoparticles used for loading include indium oxide nanopowder from U.S. Research Nanomaterials, Inc. (Houston, TX) and Degussa AG Aeroxide P25 TiO_2 (Frankfurt am Main, Germany). Fe_2O_3 NPs were synthesized by modifying a previously published method.[16] Briefly, anhydrous ferric acid (Sigma-Aldrich) was prepared over heat in a 4 mM HCl solution and 0.25 M $FeCl_3$ stock. The solution was then placed in a laboratory oven (HP 5890 series II) at 100 °C and incubated for 10 h. The Fe_2O_3 NPs were centrifuged and washed five times with nanopure water. After rinsing, the Fe_2O_3 NPs were stored at 4 °C.

In_2O_3-polymer composite, TiO_2-polymer composite, and Fe_2O_3-polymer composite solutions were prepared by dispersing various NP concentrations (0, 0.05, 0.5, and 5 wt %) in DMF by 1 h of bath sonication (Branson 2510, Branson Ultrasonic, Dansbury, CT). NP weight percentage loadings (0.05–5 wt %) into the polymers were chosen to span multiple orders of magnitude. Polymer (20 wt % of either PS or PVP) was added to the solution and gently stirred for 24 h at 40 °C.

NPs (Figure 1) were analyzed using transmission electron microscopy (TEM) and X-ray Diffraction (XRD). Five hundred particles of each material were counted by hand using ImageJ.[17] TiO_2 NPs averaged 27 ± 7 nm in size, In_2O_3 NP averaged 80 ± 17 nm, and

Fe_2O_3 averaged 46 ± 3 nm. The XRD reflections of In_2O_3 NPs are characteristic of phase-pure nanocuboids. TiO_2 was mostly anatase. Fe_2O_3 crystalline phase identification was confirmed by comparing XRD reflections with the pattern of the Joint Committee on Powder diffraction Standards database (see supporting information S1–S3).

Electrospinning

An apparatus similar to previously published electrospinning systems was constructed.[5,18–21] Briefly, electrospinning was performed using a high voltage power supply that provided up to 40 kV (Gamma High Voltage, Ormond Beach, FL), a syringe pump (New Era NE-300, Farmingdale, NY), a 10 mL plastic syringe, and a grounded aluminum foil coated collector that was placed 15 cm away from the syringe tip. The experimental procedure involved loading the solution into a plastic 10 mL syringe fitted with a stainless steel needle that was connected to the high voltage power supply. The NP-polymer composite solution was injected at 20 μL/h through a stainless steel, 22-gauge needle (Sigma-Aldrich stainless steel 304 syringe needle) with an alligator clip attached to charge the needle and the polymer solution as it exited the capillary tip. The entire system was enclosed to mitigate the effects of air currents on the system and for safety. Humidity was measured using a Xikar hygrometer and was maintained at 40% at 75 °F using a sponge saturated with deionized water inside the electrospinning enclosure. All experiments were run grouped by metal oxide on the same day in quick succession to maintain similar ambient experimental conditions.

Analytical Methods

Nanoparticles were characterized using a Philips CM200-FEG transmission electron microscope and a Siemens D5000 powder X-ray diffractometer. SEM images of fibers were obtained using a JEOL 2010F. Viscosity of polymer solutions was measured using a TA Instruments AR-G2 rheometer. Fiber diameters were measured using ImageJ software (National Institutes of Health, Washington, D.C.).

RESULTS AND DISCUSSION

Effect of Nanoparticle Doping on Critical Voltages to Produce Taylor Cones

Taylor cone formation is an important feature of the electrospinning process because it indicates that the voltage applied affects the surface tension of the solution, and because it is a precursor to a stable, continuous polymer jet. The charged jet is the distinguishing characteristic between electrospinning and electrospraying, where the end result of electrospraying is charged polymer droplets without fiber formation. The critical voltage occurs when the jet forms. Droplet shape at the tip varies with applied voltage. At lower voltages, the originating drop at the capillary tip is larger than the diameter of the capillary tip. As voltage increases, the jet originates first from the bottom of the drop, and then the drop diameter decreases with increasing voltage until the jet emerges from the solution within the syringe tip.[4] Little is known about the dependence of these voltages on NP loadings in polymers.

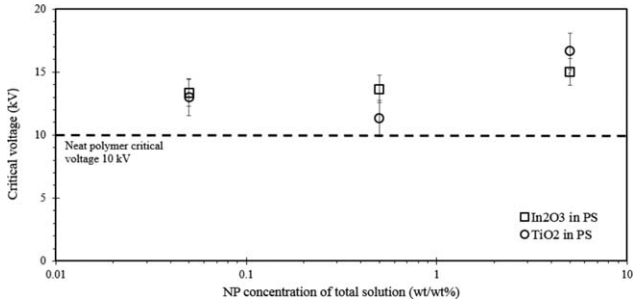

Figure 2. Critical voltage to produce a Taylor cone in PS solutions (for PVP, see SI.3). Error bars indicate 1 SD from triplicate electrospinning experiments using the same NP-polymer solution. Critical voltage applied did not change significantly until 5 wt % NP loading. This may be a product of the viscosity increase at 5 wt % NP loading (see Figure 3).

Figure 2 shows critical voltages for In_2O_3 and TiO_2 NPs at different loadings in PS. Figure S4 in supporting information shows a companion plot using PVP. For both polymers, the critical voltage did not vary for NP loadings lower than 0.5 wt %. The critical voltage needed to produce a Taylor cone without NP in solution was 10 kV. The critical voltage needed to form a stable Taylor cone increased ($p < 0.05$, Student's t test) by roughly 25% when adding up to 5 wt % TiO_2 and In_2O_3 in PS or PVP. The increase in voltage needed to form a Taylor cone may be attributed to increasing viscosity caused by NP addition. Interestingly, there was not a statistical difference ($p < 0.05$) between 0.05 and 0.5 wt % NP to increase critical voltage or polymer solution viscosity. Similar variability has been seen for small weight percentages (0–10 wt % PS NPs) in linear PS chains; the mechanism is yet to be explained.[22]

Solution viscosity can influence the voltage needed to successfully produce a polymer jet in electrospinning and also affect fiber diameter, droplet shape, and jet trajectory.[4,23] Viscosity increased ($p < 0.05$, Student's t test) with higher mass fraction of nanoparticles (Figure 3). Increasing solution viscosity requires increased voltage to produce a Taylor cone and a charged jet.[4,24] According to the Einstein-Batchelor law for spherical particle suspensions, adding particles should increase the viscosity of their host polymer.[25,26] However, this is not the case for all NP loadings. Polymer nanocomposites display a variety of unexpected behavior, most notably a reduction in viscosity.[3,22] Reduced viscosity has been observed in PS solutions containing dispersed fullerene and magnetite NPs.[27] This phenomenon has been attributed to a decrease in excluded volume due to a change in polymer conformation; the viscosity of polymer melts do not follow convention when NPs are introduced.[3,22,27]

Morphology of Nanoparticle-Polymer Fibers

Changes in viscosity are known to affect morphology of electrospun fibers.[5,6,28,29] For example, beading in polymer fibers refers to segments of polymer that are thicker than adjacent elongated fiber. Beading is usually round in nature, much like pearls on a necklace (Figure 5). Beads form in electrospun fibers due to the competition between capillary forces and electrical stress.[30] Polymer molecular weight and solution concentration have been

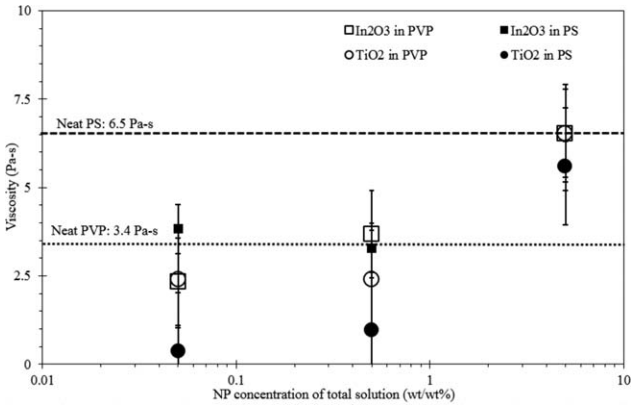

Figure 3. Viscosity of PVP and PS solutions measured using a rheometer. Error bars indicate 1 SD. Viscosity stayed constant through 0.5 wt % NP loading, and increased at 5 wt % NP loading. Addition of nanoparticles to polymer solutions is known to affect solution behavior unexpectedly; NP addition can reduce viscosity instead of increase it, as predicted by the Einstein-Batchelor law for spherical-particle suspensions.

linked to beading and branching in electrospun fibers by causing increases in solution viscosity and surface tension.[4,24,31] Fibers spun without added NPs are smooth fibers, with constant diameter thickness, and show no beading (Figure 4). In contrast, fiber morphologies with 0.05, 0.5, and 5 wt % mass fractions of In_2O_3 and TiO_2 shown in Figure 4 are not continuous fibers like those spun without NP; the NP-polymer fibers show beading and branching. These morphology changes reflect the changes in solution composition. Generally, increases in solution viscosity will cause increases in beading and other defects in electrospun fibers.[32,33] In this case, the beading observed is not detrimental for the purposes of this study.

With NP addition, fiber diameter remained constant between 1 and 3 μm (Table I). PVP solutions with no NPs had a diameter of 1.6 μm, increasing by a few microns with the addition of 0.05 wt % NPs, then decreasing by roughly half with the addition of 0.5 and 5 wt % NPs. For PS, fiber diameter was 0.8 μm without any NPs, which is consistent with the higher viscosity of PS. The PS fiber diameters double with the addition of 0.05 wt % and 0.5 wt % NPs. However, with the addition of 5 wt % NP, diameter decreased in size by roughly half ($p < 0.05$, Student's t test). Based upon what is known about spinning solutions with higher viscosity and surface tension, we believe a variation in fiber diameter of polymer solutions containing NPs was caused by the increased voltage needed to form a charged jet.[1,5,19]

Distribution of NPs in Electrospun Fibers

The distribution of NPs in fibers becomes important for certain applications, for example, when NPs in fiber function as reactive sites for sorbents.[34] In order for nanocomposite electrospun fibers to be useful, NPs must be readily accessible.[32] Figures 4–6 show NP distributions in the fibers. The 5 wt % NP-polymer solutions shown in Figure 4 are the best example of desirable distribution of NPs obtained in this study. Nanoparticle aggregates were counted manually inside 10 μm^2 areas using TEM images like those found in Figure 4 ($n = 500$ aggregates). The 5 wt % In_2O_3 shows the most uniform distribution, with an average of 6 ± 2 NP cluster/10 μm^2 area, versus 4 ± 1 cluster/10 μm^2 area for 5 wt % TiO_2. EDX analysis confirmed indium and titanium presence in electrospun fibers observed utilizing backscatter SEM imaging (Figure 5). Figure 5 also shows magnified images of PVP fibers with 1 wt % In_2O_3 added, which formed both polymer beads and aggregated In_2O_3 beads. NP aggregations may occur due to polymer-nanoparticle interactions, as well as electrostatic forces between the nanoparticles themselves. NP distributions in polymers are not well understood; this is due to a lack of theoretical studies, systematic experimental results, and the challenges of processing nanocomposites.[35] Existing literature reports suggest a lack in consensus on a single quantitative method for the evaluation of the state of dispersion of nanoparticles in suspensions. Khare *et al.* proposed a method for obtaining free space length (L_f).[36] L_f is described as the characteristic size of unreinforced polymer domains within nanoparticle suspensions. By quantifying the size of these unreinforced particle domains, dispersion states can be distinguished between polymer suspensions. L_f is reduced as a product of more uniform dispersion, decreasing particle size, and increased nanoparticle loading.[36] The L_f of a 5% TiO_2 suspension before and after spinning was found using the TEM images shown in Figure 6 in accordance with the previously published method.[36] The L_f of 5% TiO_2 in PS before spinning was 161 ± 16 nm, while that of 5% TiO_2 in PS after spinning was 155 ± 6 nm. Changes in the state of dispersion of NPs can influence electrospinning performance; in this case, the state of dispersion of the TiO_2 suspensions in polystyrene was similar before and after spinning despite the method of data interpretation.

Table I. Effect of NP Loading and Polymer on Electrospun Fiber Diameter

	Fiber diameter (μm ±1 SD)			
Sample	No. NP	0.05 wt % NP	0.5 wt % NP	5 wt % NP
In_2O_3 in PVP	1.6 ± 0.25	1.93 ± 0.53	0.59 ± 0.15	0.81 ± 0.23
TiO_2 in PVP	1.6 ± 0.25	1.75 ± 0.41	0.68 ± 0.20	0.83 ± 0.35
In_2O_3 in PS	0.81 ± 0.20	1.9 ± 0.43	1.8 ± 0.52	0.82 ± 0.20
TiO_2 in PS	0.81 ± 0.20	1.45 ± 0.53	3.8 ± 1.8	0.72 ± 0.48

Average diameter of fiber to 1 SD. Measurements were made in triplicate. PVP solutions showed no effect with 0.05 wt % NP addition, and then a reduction in half of fiber diameter by addition of 0.5 and 5 wt % NP. PS with no NP addition had a lower fiber diameter, which is consistent with the higher viscosity of PS. Adding 0.05 wt % NP significantly increased fiber diameter, but was unchanged at highest NP loading of 5 wt %.

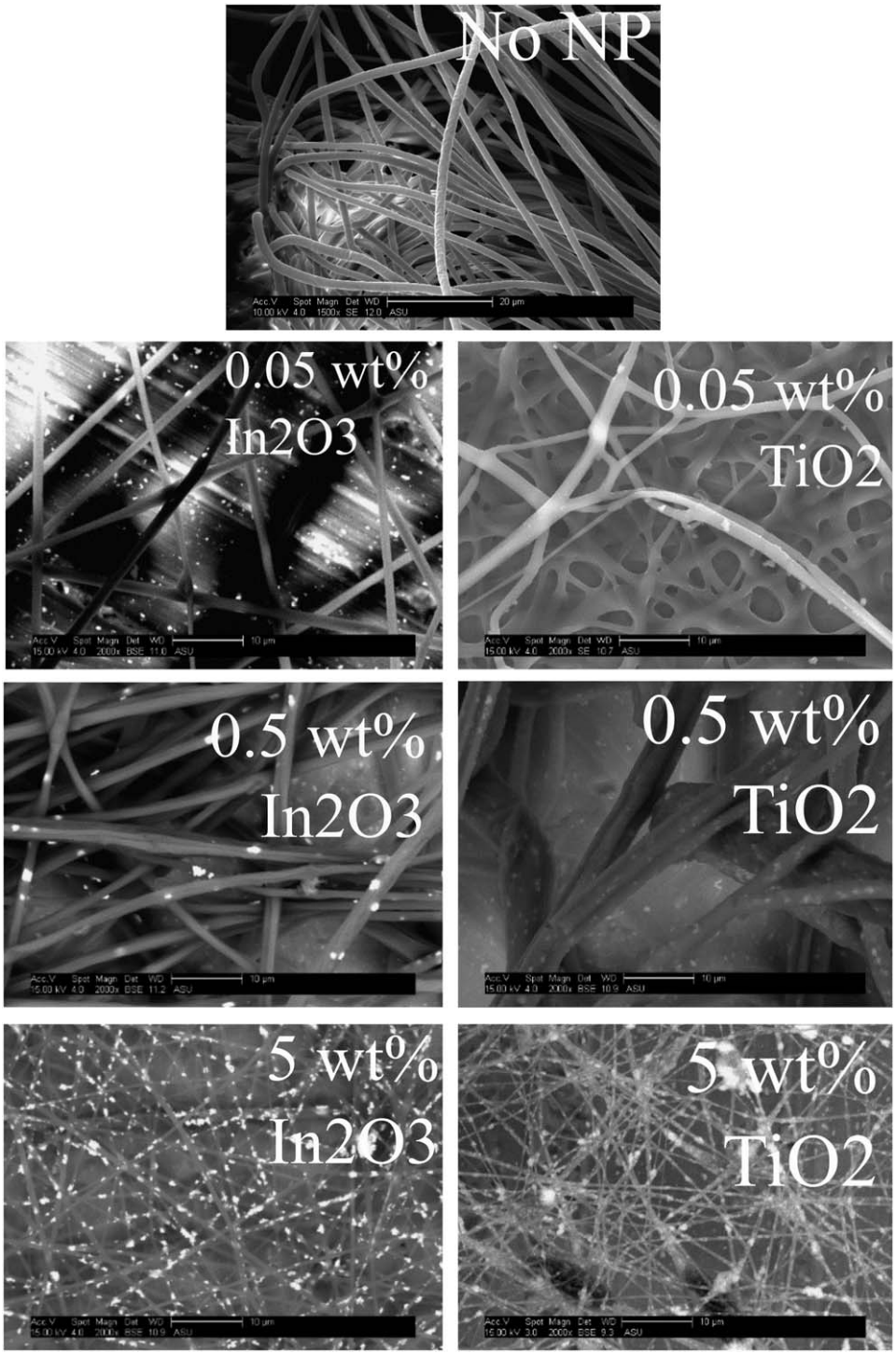

Figure 4. SEM images of PS fibers with In_2O_3 and TiO_2. Fibers with no NP added are smooth and continuous. NP addition increases beading and branching. Backscatter mode shows that NPs are evenly distributed in fibers.

In addition to assessing the state of dispersion of 5% TiO_2 in PS, the particle size distributions of this suspension were evaluated. Particles were manually counted and measured using ImageJ (n = 500 particles). Figure 7 shows the particle sizes distributions for loose TiO_2 NPs, 5% TiO_2 in PS prior to spinning, and 5% TiO_2 in PS after spinning. The figure indicates that between the three phases of the experiment the NPs were in the 10–20 nm range in size and could not exert effects on nanoparticle dispersion or electrospinning performance by changing diameter. Coupled with the uniformity of state of dispersion throughout the experiment, these results indicate little to no influence on electrospinning performance by interactions

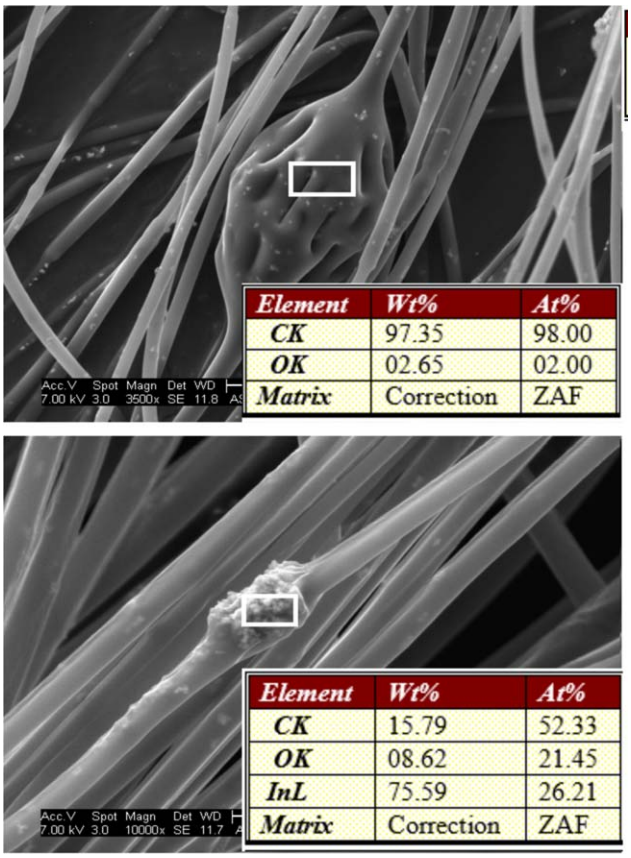

Figure 5. Images of 1 wt % In_2O_3 in PVP. Beading is common in electrospun fibers. A polymer bead with In_2O_3 nanoparticles in it (top) as well as an aggregate of In_2O_3 NPs (bottom) is shown. [Color figure can be viewed in the online issue, which is available at wileyonlinelibrary.com.]

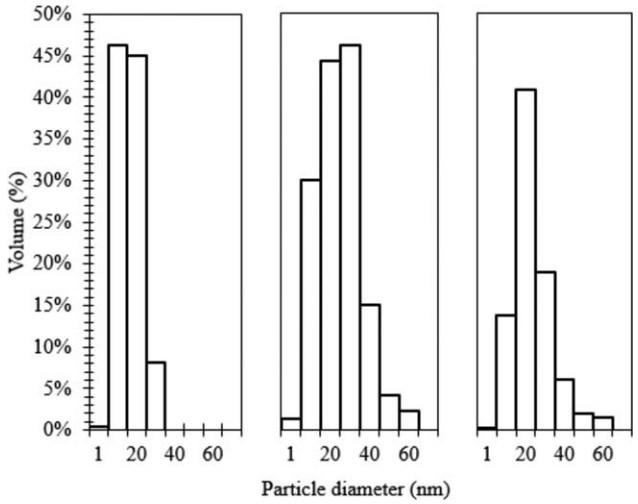

Figure 7. Particle size distributions (n = 500) of TiO_2 NP for (left to right) loose TiO_2 particles, 5% TiO_2 in PS suspension prior to spinning, and 5% TiO_2 in PS suspension after spinning. The majority of the NPs were in the 10–20 nm range for all treatments.

of nanoparticles with the polymer matrix or within the nanoparticle aggregates. The nanoparticles formed aggregates as soon as they were suspended, despite sonication, and maintained their state through the experiment.

Figure 8 shows SEM magnifications of Fe_2O_3 in PS. Fe_2O_3 NPs were added to PS solution for comparison against TiO_2 and In_2O_3. Electrospinning is based on the manipulation of charge. Nanoscale Fe_2O_3 is highly conductive, displays behavior unique to nanoparticles, and may behave differently in the electrospinning system. Similar with TiO_2 and In_2O_3, the Fe_2O_3 nanoparticles are

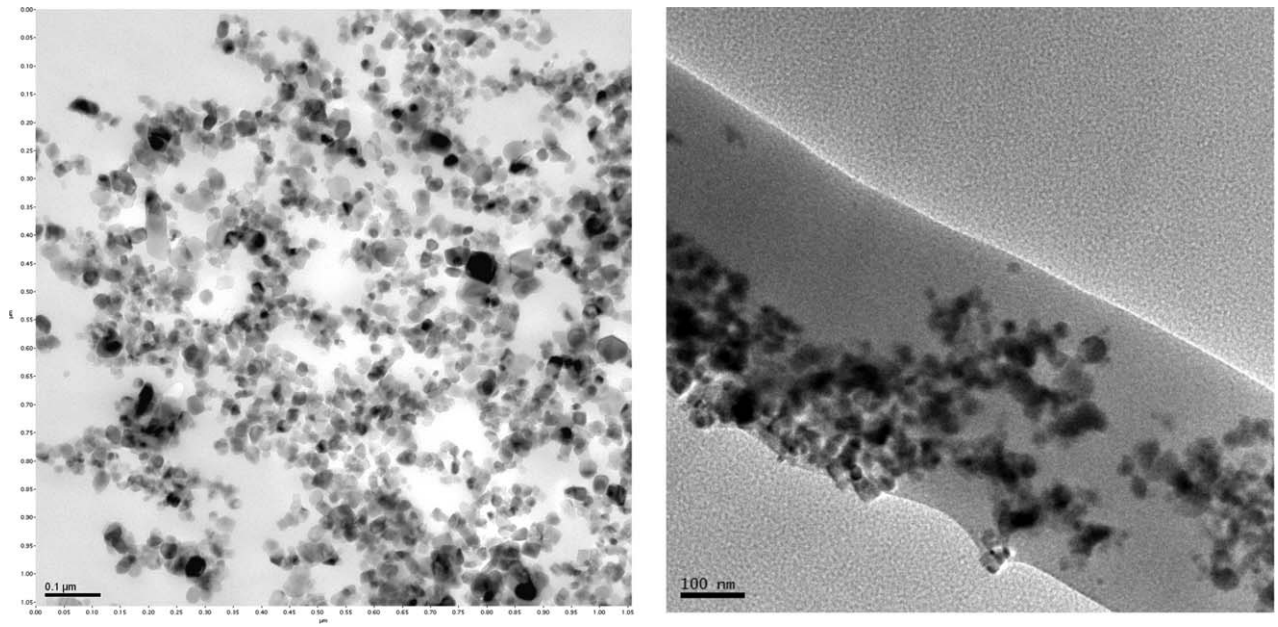

Figure 6. Five percent **of** TiO_2 in PS before electrospinning (top) and after electrospinning (bottom). The free length (L_f) of the suspension as specified in Khare *et al.* was found to be 161 ± 16 nm before spinning and 155 ± 6 nm after spinning. The state of dispersion of the TiO_2 suspensions in polystyrene was similar before and after spinning despite the method of data interpretation.

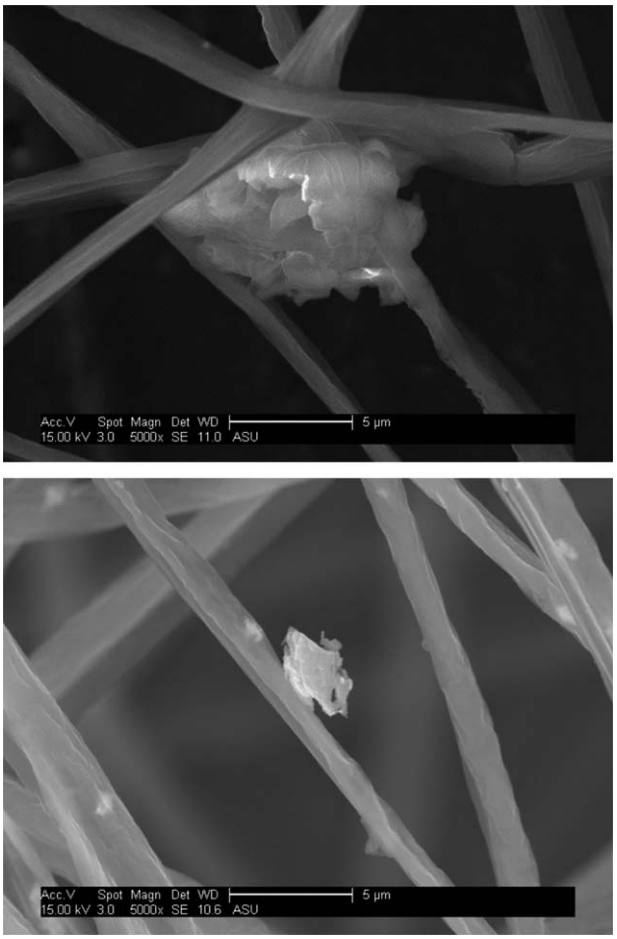

Figure 8. 0.05 wt % (top) and 0.5 wt % Fe_2O_3 (bottom) in PS. Both images show polymer defects, a common occurrence in electrospinning. 0.5 wt % Fe_2O_3 shows discernible flecks, which are the Fe_2O_3 NP distributed in the fiber itself.

discernible at 0.5 wt % in the fiber, and are well distributed through the polymer filament.

Demonstration of Adsorption by a TiO_2-PS Composite Fiber

A motivation for the experiments detailed in this paper was to effectively harness the potential benefits of suspending nanoparticles such as TiO_2 in a polymer scaffold in order to facilitate their use as active sites for remediation processes, such as adsorption. The aim was to make a hybrid NP-polymer fiber in a single step, without posttreatment (e.g., attachment of NP after spinning a polymer fiber, calcination of a nonpolymeric metal sol). Our control experiments with TiO_2 alone in water confirmed literature reports demonstrating its ability to remove As(V).[37] Therefore, a single-point arsenate [As(V)] adsorption experiment was conducted using a hybrid NP-polymeric fiber created from a dispersion of 5 wt % TiO_2 in polystyrene and DMF. With the incorporation of TiO_2 in the fiber, sorption of As(V) was expected; however, upon experimentation, no As(V) sorbed onto the composite fiber. We hypothesized that while TiO_2 is well dispersed in the polymeric fiber, the fiber was smooth and all measurements indicated that it was nonporous. Separately, recent work (Hoogesteijn von Reitzenstein *et al.*, in preparation) shows that dispersing graphene platelets in PS/DMF prior to electrospinning created fibers with surface porosity. These pores provide access points between the aqueous phase and the graphene embedded within the polymeric fibers. Therefore, we spun a hybrid NP-polymeric fiber by dispersing both TiO_2 and graphene together in PS/DMF. The resulting fibers are porous (Figure 9), but did not adsorb As(V). To prove the porosity could allow sorption of pollutants by NPs within the polymeric fiber adsorption experiments using a nonpolar organic pollutant [phenanthrene ($C_{14}H_{10}$)] confirmed >50 times more adsorption on the hybrid fiber than a polymer-only (control) fiber (no NP). The phenanthrene sorption, on a mass removal basis (mg phenanthrene per g graphene) is equivalent between a dispersion of graphene in water (no fiber) and the hybrid NP-polymer fiber, thus proving the organic pollutant adsorbs only to the graphene and that the graphene NP surface is available within the pores of the fiber for phenanthrene. We suspect that the lack of As(V) sorption in the hybrid TiO_2/graphene-polymer fiber was not due to the lack of pore formation

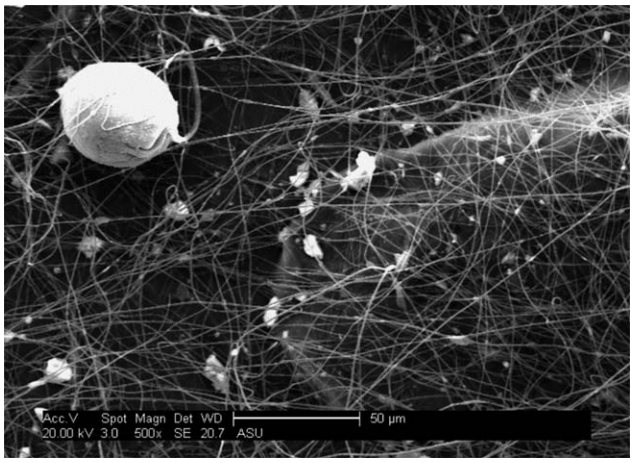

Figure 9. SEM image of a 5 wt % TiO_2−1 wt % graphene platelet PS fiber bead. The TiO_2-graphene composite fiber did not show sorption of As(V).

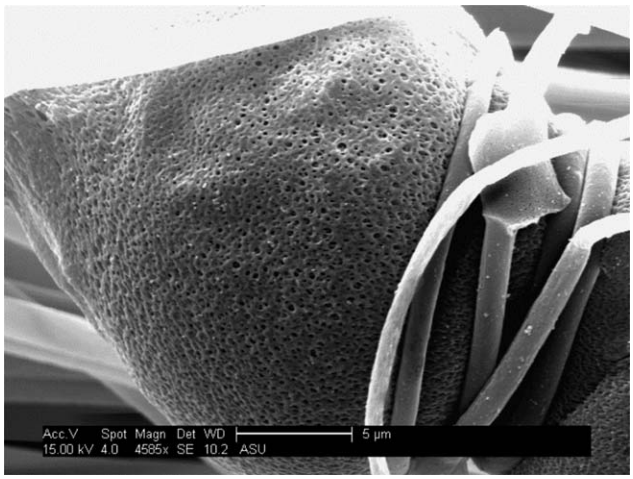

Figure 10. SEM image of a 5 wt % graphene platelet PS fiber. Pores are clearly visible. Graphene composite fibers have shown a 225 mg/g adsorption capacity for phenanthrene.

but rather that the polymer still encompassed the TiO_2 NP within the fiber. A way to create pores and allow connectivity between As(V) in water and TiO_2 could be to use new TiO_2-graphene nanoparticles. Multifunctional TiO_2-graphene composite nanomaterials have been synthesized with TiO_2 encapsulated within crumpled graphene sheets.[38,39] These types of materials may provide a one-step method to synthesize water-stable hybrid NP-polymeric fibers and nonwoven textiles capable of pollutant removal from water.

CONCLUSIONS

This study investigated the effect of NP addition on electrospun polymer fibers and how viscosity, critical voltage, and fiber morphology changed as a result. Viscosity and critical voltage increased with increasing weight percentage of nanoparticles in the polymer solution. Critical voltage needed to produce a Taylor cone was higher for PS than for PVP. Fiber morphology was not directly affected by NP addition; instead the increase in viscosity and higher surface tension as a result of the 5 wt % NP concentration caused a roughly 50% decrease in diameter. Taking higher critical voltages and viscosities into account when adding NPs to polymer solutions has implications for future electrospinning applications, specifically for applications where fiber diameter and surface morphology are important. While even distribution of NP was observed, it is important to sonicate electrospinning solutions containing NP to prevent aggregation. The voltage changes needed to successfully spin higher weight percentages of NP-polymer composites can affect this technology's the scale up process, including the power required to produce such fibers. Finally, NP weight percentage significantly affected the number of reactive sites available for NP functionality. Special attention needs to be paid to experimental parameters and solution composition in order to optimize fiber production. Overall, TiO_2 and In_2O_3 NPs can be successfully integrated into electrospun fibers with adjustments to voltage based on NP concentration in polymer solution. The potential for high surface area, low volume, functionalization capability, and ease of synthesis make electrospun fibers good candidates for water treatment applications such as nanofiltration and ion exchange. Further work should focus on functionalizing electrospun fibers with embedded NPs for water treatment purposes.

ACKNOWLEDGMENTS

The authors gratefully acknowledge David Lowry, Jared Schoepf, Pierre Herckes, Tyler Harris, Stella Nickerson, and Lenore Dai. We gratefully acknowledge the use of facilities with the LeRoy Eyring Center for Solid State Science at Arizona State University. The authors would like to thank the Arizona State University Ira A. Fulton Schools of Engineering Dean's Fellowship program, National Water Research Institute, the National Science Foundation (Graduate Research Fellowship Program grant number DGE-1311230) and United States Environmental Protection Agency (grant number RD835580), and Science Foundation Arizona for supporting this work. This work was also partially funded through the Nano-Enabled Water Treatment Technologies Nanosystems Engineering Research Center by the National Science Foundation (EEC-1449500).

REFERENCES

1. Huang, Z. M.; Zhang, Y. Z.; Kotaki, M.; Ramakrishna, S. *Compos. Sci. Technol.* **2003**, *63*, 2223.
2. Li, D.; Xia, Y. *Adv. Mater.* **2004**, *16*, 1151.
3. Mangal, R.; Srivastava, S.; Archer, L. A. *Nat. Commun.* **2015**, *6*, 1–9.
4. Deitzel, J. M.; Kleinmeyer, J.; Harris, D.; Tan, N. C. B. *Polymer* **2001**, *42*, 261.
5. Casper, C. L.; Stephens, J. S.; Tassi, N. G.; Chase, D. B.; Rabolt, J. F. *Macromolecules* **2004**, *37*, 573.
6. Medeiros, E. S.; Mattoso, L. H. C.; Offeman, R. D.; Wood, D. F.; Orts, W. J. *Can. J. Chem.* **2008**, *86*, 590.
7. Ramakrishna, S.; Fujihara, K.; Teo, W. E.; Lim, T. C. *J. Eng. Fibers Fabr.* **2008**, *3*, 46.
8. Li, Y.; Gong, J.; He, G.; Deng, Y. *Mater. Chem. Phys.* **2011**, *129*, 477.
9. Su, C.; Ran, X.; Hu, J.; Shao, C. *Environ. Sci. Technol.* **2013**, *47*, 11562.
10. Ramaseshan, R.; Sundarrajan, S.; Jose, R.; Ramakrishna, S. *J. Appl. Phys.* **2007**, *102*, 111101.
11. Xu, X.; Yang, Q.; Wang, Y.; Yu, H.; Chen, X.; Jing, X. *Eur. Polym. J.* **2006**, *42*, 2081.
12. Li, D.; Xia, Y. *Nano Lett.* **2003**, *3*, 555.
13. Ding, B.; Kim, C. K.; Kim, H. Y.; Seo, M. K.; Park, S. *J. Fibers Polym.* **2004**, *5*, 105.
14. Madani, M.; Sharifi-Sanjani, N.; Hasan-Kaviar, A.; Choghazardi, M.; Faridi-Majidi, R.; Hamouda, A. S. *Polym. Eng. Sci.* **2013**, *53*, 2407.
15. Caruso, R. A.; Susha, A.; Caruso, F. *Chem. Mater.* **2001**, *13*, 400.
16. Matijević, E.; Scheiner, P. *J. Colloid Interface Sci.* **1978**, *63*, 509.
17. Schindelin, J.; Arganda-Carreras, I.; Frise, E.; Kaynig, V.; Longair, M.; Pietzsch, T.; Preibisch, S.; Rueden, C.; Saalfeld, S.; Schmid, B.; Tinevez, J. Y. J. Y.; White, D. J.; Hartenstein, V.; Eliceiri, K.; Tomancak, P.; Cardona, A.; Liceiri, K.; Tomancak, P. A. C. *Nat. Methods* **2012**, *9*, 676.
18. Fong, H.; Chun, I.; Reneker, D. H. *Polymer (Guildf)* **1999**, *40*, 4585.
19. Leach, M. K.; Feng, Z. Q.; Tuck, S. J.; Corey, J. M. *J. Vis. Exp.* **2011**.
20. Thavasi, V.; Singh, G.; Ramakrishna, S. *Energy Environ. Sci.* **2008**, *1*, 205.
21. Yang, Q.; Li, Z.; Hong, Y.; Zhao, Y.; Qiu, S.; Wang, C.; Wei, Y. *J. Polym. Sci. Part B* **2004**, *42*, 3721.
22. Mackay, M. E.; Dao, T. T.; Tuteja, A.; Ho, D. L.; van Horn, B.; Kim, H. C.; Hawker, C. *J. Nat. Mater.* **2003**, *2*, 762.
23. Doshi, J.; Reneker, D. H. *J. Electrostat.* **1995**, *35*, 151.
24. Eda, G.; Liu, J.; Shivkumar, S. *Mater. Lett.* **2007**, *61*, 1451.
25. Batchelor, G. K. *J. Fluid Mech.* **1970**, *41*, 545.
26. Einstein, A. *Ann. Phys.* **1905**, *322*, 549.
27. Tuteja, A.; Duxbury, P. M.; Mackay, M. E. *Macromolecules* **2007**, *40*, 9427.
28. Ojha, S. S.; Afshari, M.; Kotek, R.; Gorga, R. E. *J. Appl. Polym. Sci.* **2008**, *108*, 308.

29. Pai, C. L.; Boyce, M. C.; Rutledge, G. C. *Macromolecules* **2009**, *42*, 2102.
30. Balgis, R.; Kartikowati, C. W.; Ogi, T.; Gradon, L.; Bao, L.; Seki, K.; Okuyama, K. *Chem. Eng. Sci.* **2015**, *137*, 947.
31. Lee, K. H.; Kim, H. Y.; Bang, H. J.; Jung, Y. H.; Lee, S. G. *Polymer (Guildf)* **2003**, *44*, 4029.
32. Patel, A. C.; Li, S.; Wang, C.; Zhang, W.; Wei, Y. **2007**, *120*, 12289.
33. Mazinani, S.; Ajji, A.; Dubois, C. *Polymer (Guildf)* **2009**, *50*, 3329.
34. Tran, D.; Marti, A.; Balkus, K. *Fibers* **2014**, *2*, 308.
35. Jordan, J.; Jacob, K. I.; Tannenbaum, R.; Sharaf, M. A.; Jasiuk, I. *Mater. Sci. Eng. A* **2005**, *393*, 1.
36. Khare, H. S.; Burris, D. L. *Polymer (Guildf)* **2010**, *51*, 719.
37. Dutta, P. K.; Ray, A. K.; Sharma, V. K.; Millero, F. J. *J. Colloid Interface Sci.* **2004**, *278*, 270.
38. Jiang, Y.; Wang, W. N.; Biswas, P.; Fortner, J. D. *ACS Appl. Mater. Interfaces* **2014**, *6*, 11766.
39. Jiang, Y.; Wang, W. N.; Liu, D.; Nie, Y.; Li, W.; Wu, J.; Zhang, F.; Biswas, P.; Fortner, J. D. *Environ. Sci. Technol.* **2015**, *49*, 6846.